ELSEVIER

Journal of Magnetism and Magnetic Materials 164 (1996) 241–250

journal of magnetism and magnetic materials

# Size and structural effects on the magnetic behaviour of $Gd_2CuO_4$ particles

J. Mira [a,*], J. Rivas [a], D. Fiorani [b], R. Caciuffo [c], D. Rinaldi [c], C. Vázquez Vázquez [d], J. Mahía [d], M.A. López Quintela [d], S.B. Oseroff [e]

[a] *Departamento de Física Aplicada, Universidade de Santiago, E-15706 Santiago de Compostela, Spain*
[b] *Istituto di Chimica dei Materiali-Consiglio Nazionale delle Ricerche, I-00016 Monterotondo Stazione, Roma, Italy*
[c] *Dipartimento di Scienze dei Materiali e della Terra, Universitá di Ancona, 60131 Ancona, Italy*
[d] *Departamento de Química-Física, Universidade de Santiago, E-15706 Santiago de Compostela, Spain*
[e] *Physics Department, San Diego State University, San Diego, CA 92182, USA*

Received 22 January 1996; revised 17 April 1996

**Abstract**

The magnetic properties of $Gd_2CuO_4$, synthesized by ceramic and sol–gel methods, have been investigated by dc and ac susceptibility measurements. Both static and dynamic properties have been found to depend on the synthesis temperature for ceramic samples, and on the particle size for sol–gel ones. The role of structural and size effects on the observed changes is discussed.

*PACS:* 75.60.Jp; 75.60.Nt

*Keywords:* Magnetic irreversibilities; Fine particles; Size effects; Synthesis–temperature effects; Weak ferromagnetism

## 1. Introduction

The rare earth cuprates $R_2CuO_4$, R = lanthanide, are the basis compounds of the high-$T_c$ superconductors $R_{2-x}(Th,Ce)_xCuO_4$ (R = Pr, Nd, Sm, Eu) [1]. All of them, but $La_2CuO_4$, crystallize in the tetragonal T′ phase [2], although for R = Tb and heavier rare earths can only be prepared under pressure [3]. They are characterized by the presence of $CuO_2$ planes with long range antiferromagnetic (AF) ordering of the magnetic moments of the $Cu^{+2}$ ions [4], with a coupling constant $J > 1000$ K [5,6]. Such a high value makes possible the existence of 2D spin correlated regions within the planes at high temperatures. The size of these regions increase as the temperature decreases, until a crossover to a global 3D ordering takes place at a temperature, $T_N$, between 260–280 K [6,7]. Below this temperature, for R = Gd and heavier rare earths, a weak ferromagnetic (WF) component appears in the antiferromagnetically coupled lattice [8]. This fact is coincident with the non-appearance of superconductivity in these materials upon Th or Ce doping [9], what has resulted in an increase on the interest of the study of their magnetic properties to understand the disap-

* Corresponding author. Email: fajmirap@usc.es; fax: +34-81-520676.

0304-8853/96/$15.00 Copyright © 1996 Elsevier Science B.V. All rights reserved.
*PII* S0304-8853(96)00359-9

pearance of superconductivity in the WF compounds. In particular, $Gd_2CuO_4$ occupies a special place because of being the only WF compound of the series which can be obtained at normal pressures.

The occurrence of WF has been attributed to a Dzyaloshinskii–Moriya antisymmetric exchange interaction [10]

$$H_{ij}^{DM} = \boldsymbol{D}\left[\boldsymbol{S}_i \times \boldsymbol{S}_j\right] \quad (1)$$

between nearest neighbours, $\boldsymbol{S}_i$ and $\boldsymbol{S}_j$, in the $CuO_2$ planes. However, in the case of the T′ structure the Dzyaloshinskii–Moriya vector $\boldsymbol{D}$ vanishes, and a coherent structural distortion is necessary for the appearance of WF. An extensive investigation of several $(R,R')_2CuO_4$ solid solutions supports a boundary for WF in these cuprates associated with the size of the planar $CuO_2$ lattice at a value $a = 3.910$ Å, that corresponds to $Eu_2CuO_4$ [8,11]. The boundary for WF is associated with a displacement of the oxygen atoms within the $CuO_2$ planes, O(1), from their symmetric position [12]. In fact, superstructure reflections observed by neutron diffraction reveal a rotation around the $c$-axis of the O(1) squares surrounding the Cu sites [13]. The sign of the corresponding WF moments is determined by the direction of the O(1) displacements. This implies that a certain coherence of the O(1) distortions is necessary in order to have a macroscopic WF [14]. The thermal treatment dependence of the dynamic magnetic behaviour of $Gd_2CuO_4$ [15] has suggested that the coherence of the O(1) distortions could be altered through the treatment temperature, enabling the existence of planar WF domains.

On the other hand, a direct reduction of particle size by sol–gel methods has shown very interesting effects on the dynamic magnetic properties of the material [16]. In this paper we analyze the changes on the magnetic properties of $Gd_2CuO_4$, considering the role that structural and size effects are playing both in ceramic and sol–gel samples.

## 2. Experimental details

### 2.1. Sample synthesis

The ceramic samples were synthesized by conventional solid state reaction, using $Gd_2O_3$ and CuO oxides as starting materials, at several temperatures. Stoichiometric amounts of the oxides were ground for several hours and, for the so called sample C1, thermal treated at 850°C with frequent intermediate grindings. Around 400 h were required to obtain the pure phase. Another ceramic sample, named C2, was prepared in several steps with intermediate grindings at a synthesis temperature of 1080°C.

For the sol–gel technique, using urea as gelificant agent, nitrate salts were used as starting materials, due to their high solubility in water. The solvent was evaporated on a hot plate with continuous stirring. When cooling, a gel is formed which is decomposed in an oven at 250°C, yielding the precursor of these samples. After grinding the precursor, it was submitted to several annealings at different temperatures, from 600 (sample S5) to 950°C (sample S1), in order to obtain particles of different sizes. Details of this process have been previously reported [17].

### 2.2. Experimental techniques

The polycrystalline powders were characterized analyticaly by Inductive Coupled Plasma Atomic Emission Spectroscopy (ICP-AES), using an ICP Perkin-Elmer 5000 with Ar plasma. The structural characterization was carried out by X-ray Powder Diffraction, using a diffractometer Philips PW-1710 with Cu anode. X-ray diffraction measurements were performed at room temperature. In order to determine the size distribution, investigations by Photon Correlation Spectroscopy (PCS), transmission electron microscopy (TEM) and scanning electron microscopy (SEM) were carried out. The PCS measurements were performed with an Ar laser Liconix series 5000 of 5 W operating at $\lambda = 488$ nm and a goniometer ALV-SP80 controlled automatically by means of an ALV-LSE unit. For those measurements, particles were dispersed in ethylene glycol using Triton X-100 as dispersing agent.

The dc magnetic measurements were carried out using a Quantum Design SQUID and a DMS-1660 Vibrating Sample Magnetometer in the temperature range $4\ \mathrm{K} < T < 300\ \mathrm{K}$. The real and imaginary part components $\chi'$ and $\chi''$ of the external complex ac susceptibility were measured as a function of temperature using a mutual inductance technique described elsewhere [15]. The calibration was per-

formed using a $Gd_2(SO_4)_3 \cdot 8H_2O$ paramagnetic standard with the same shape and size as the investigated samples. Demagnetizing effects have been taken into account in the calculation of the so called internal susceptibility. Data were collected on warming from 13 to 300 K, after zero field cooling of the sample. For each run of measurements, the ac field was applied with a fixed amplitude of $H_{ac} = 300$ A/m (3.75 Oe) at fixed frequencies $f$, ranging from 5 to 1000 Hz. A dc field, $H_{dc}$ from 0 to 800 A/m (10 Oe), was generated by applying a dc current to the primary coil. The temperature of the samples was controlled with an accuracy of about 0.1 K.

### 2.3. Structural and size characterization

For ceramic samples obtained by solid state reaction, X-ray diffraction indicates a pure $Gd_2CuO_4$ phase. By means of gravimetric pyrolysis it was determined that the proportion of C, H, and N in the final sol–gel samples is lower than the detection limit of this technique. This indicates that the urea decomposes almost completely and does not contaminate the final samples. The results from ICP measurements show that the molar ratio Gd/Cu is $2.1 \pm 0.1$, i.e. the stoichiometry of the starting solutions is kept in the final samples. X-ray diffraction data for the sol–gel samples show that the time necessary to obtain the right phase decreases considerably as the calcination temperature increases (see Table 1). A pure $Gd_2CuO_4$ phase is not obtained at low temperatures, the presence of the initial oxides, $Gd_2O_3$ and CuO was found. The percentage of the correct phase (within an error of 5%) increases with higher calcination temperatures as seen in Table 1. The presence of such oxides has been proved to have non-important effects on the measured temperature dependence of the magnetic properties. The Rietveld refinement of the spectra shows no changes for the ceramic samples and a slight increase of the lattice parameters in the sol–gel samples (see Table 1). A detailed analysis has been recently reported [18]. This point is crucial due to the influence of the $a$

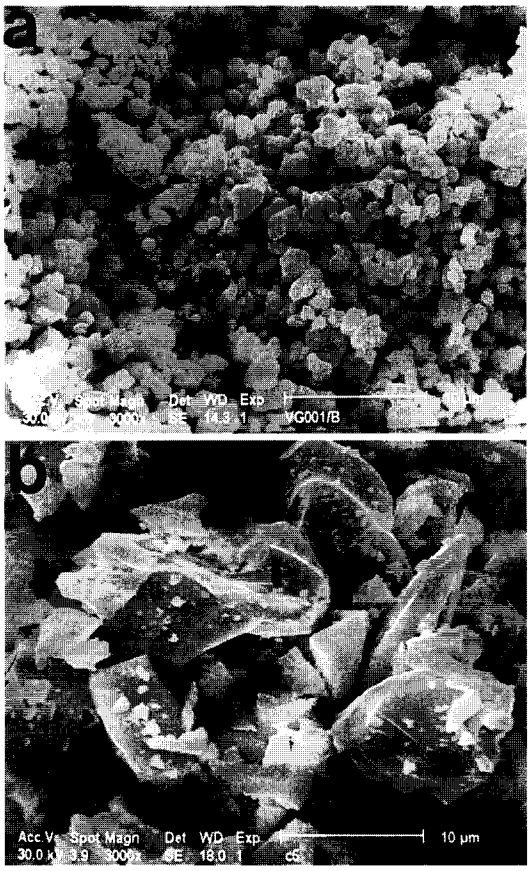


Fig. 1. SEM images obtained on selected specimens of the investigated ceramic samples. The average grain sizes are $1530 \pm 650$ nm for sample C1, annealed at 850°C (a) and $11700 \pm 7400$ nm for sample C2, annealed at 1080°C (b).

Table 1
Synthesis conditions, purity, Cu–O(1)–Cu distance and mean particle size for the sol–gel samples

| Sol–gel samples | Calcination time | Calcination temperature (°C) | $Gd_2CuO_4$ (%) | $a$ (Å) | Size (nm) |
|---|---|---|---|---|---|
| S1 | 3 h | 950 | > 95 | 3.894(1) | $350 \pm 60$ |
| S2 | 3 h | 850 | > 95 | 3.894(1) | $270 \pm 40$ |
| S3 | 6 h | 800 | > 95 | 3.895(1) | $200 \pm 30$ |
| S4 | 50 h | 650 | 90 | 3.896(1) | $110 \pm 20$ |
| S5 | 50 h | 600 | 85 | 3.896(1) | $85 \pm 20$ |

parameter on the magnetic properties of the $R_2CuO_4$ family. In our case the maximum $a$ parameter observed, 3.896(1) Å, is relatively far from the value 3.910 Å quoted as the boundary for WF. In Fig. 1 we show SEM micrographs of the ceramic samples. It can be seen a large polydispersity as well as a certain reduction of their mean size with the synthesis temperature, going from $1530 \pm 650$ nm for sample C1 to $11700 \pm 7400$ nm for sample C2. In Table 1 it is shown the evolution of the average size for samples prepared via sol–gel techniques versus final calcination temperature, obtained by TEM. As it can be seen the particle size increases with the annealing temperature. The data are in agreement with those obtained by PCS, which also shows that the size distribution is reasonably monodisperse.

## 3. Magnetic results

In Fig. 2 we show the dc and ac magnetic susceptibilities for sample C2, which will be used as the reference for the bulk material. The two main features which can be observed are associated with WF [19]. The maximum for $\chi'$ and dc magnetization at $T_l = 20$ K has been suggested to be related to a spin reorientation transition of the Cu sublattice due to the increase of the Gd–Cu interaction at low temperatures [8,14,19]. The one at $T_h = 280$ K reveals the 3D order of the Cu sublattice, whose WF component polarizes the $Gd^{3+}$ ion [20]. When measuring C1 some changes above $\sim 200$ K are found (Fig. 3). However, at low temperatures the response is similar for both the dc and ac susceptibilities. For example, the change in dc magnetization at $T_h$ is not as abrupt and the splitting temperature between field cooled (FC) and zero field cooled (ZFC) magnetizations, $T_B$, happens at lower $T$. This point is marked also by a maximum in $\chi'$, quite larger than in C2, at a temperature $T_M \simeq T_B$, that shifts from $\sim 280$ K for C2 to 210 K for C1. The FC state behaves as a metastable one. A slow magnetic relaxation process has been found between the FC and the stable ZFC state [21,22]. The ac susceptibility for sample C1 is strongly frequency dependent, unlike C2 [15]. The frequency sensitivity (estimated from the slope of the straight line in the $\chi'$ versus $\ln f$ plot at constant temperature) goes through a maximum between 100

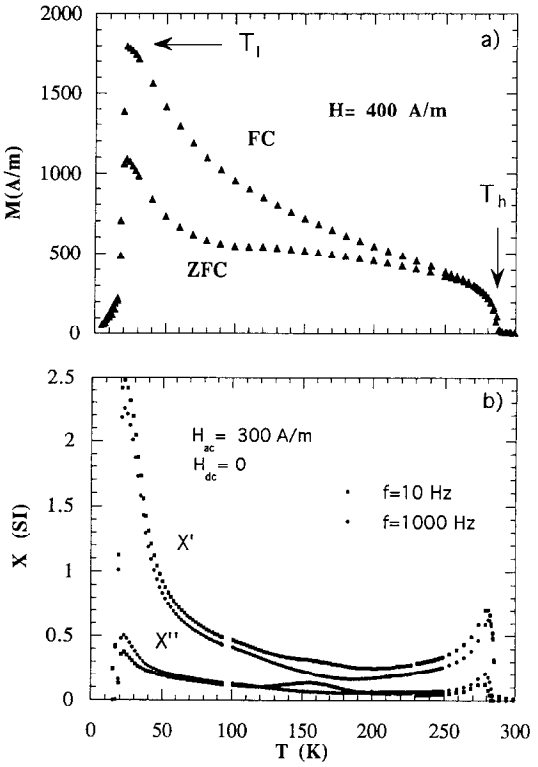


Fig. 2. (a) Dc magnetization for ceramic sample C2 at a field of 400 A/m (5 Oe). (b) Real ($\chi'$) and imaginary ($\chi''$) parts of the internal ac susceptibility measured with an ac amplitude $H_{ac} = 300$ A/m (3.75 Oe) and frequencies of $f = 10$ Hz and $f = 1000$ Hz.

and 200 K. Moreover, contrary to sample C2, $T_M$ is also frequency dependent, shifting to higher values with increasing frequency. The variations of both $T_B$ and the hight of the $\chi'$ maximum in the intermediate ceramic samples are monotonic between these two extremes. The application of a dc magnetic field induces a small shift of $T_B$, but strongly reduces the amplitude of the peak, which is almost suppressed by a field of about 800 A/m (10 Oe) in C2 and C1 (Fig. 4).

Detailed measurements taken with a temperature step of 0.1 K reveal a double peak structure of the 20 K anomaly, with a second peak at 18.5 K and a local minimum at 19 K. The temperature of both maxima does not depend on the frequency. The results obtained for sample C1 are shown in Fig. 5a; the ac susceptibility is depressed by a small amount when increasing the frequency and the intensity of the dc magnetic field, with the double peak structure still

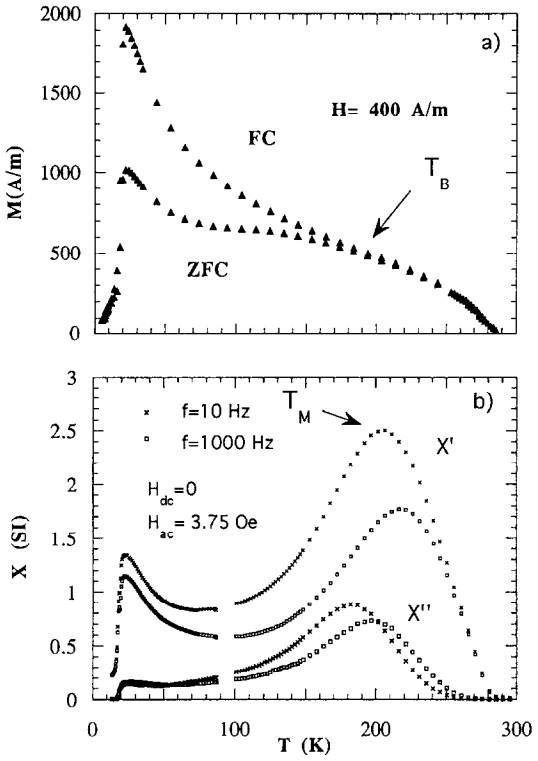


Fig. 3. (a) Dc magnetization for ceramic sample C1 at a field of 400 A/m (5 Oe). (b) Real ( $\chi'$ ) and imaginary ( $\chi''$ ) parts of the internal ac susceptibility measured with an ac amplitude $H_{ac}$ = 300 A/m (3.75 Oe) and frequencies of $f$ = 10 Hz and $f$ = 1000 Hz.

present for $H_{dc}$ = 800 A/m (10 Oe) (see inset). Below 17 K the dynamic effects become very small and the susceptibility no longer is dependent on the

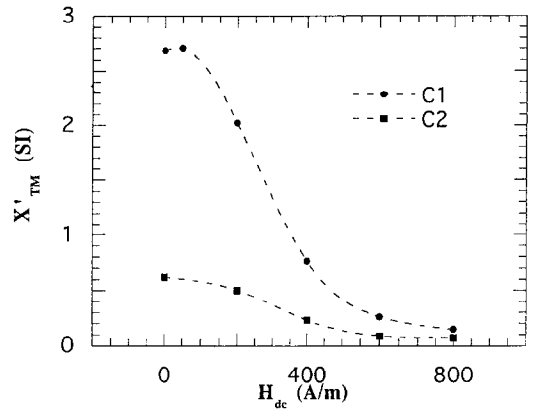


Fig. 4. Dependence of the maximum of $\chi'$ at $T_M$ on the amplitude of an external dc magnetic field for samples C1 and C2.

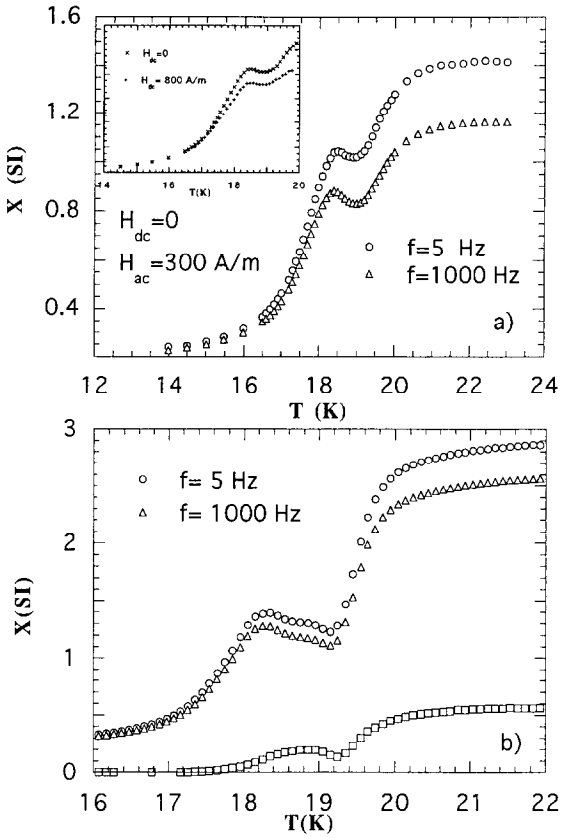


Fig. 5. Detail, at low temperatures, of the real part of the ac magnetic susceptibility measured for samples C1 (a) and C2 (b) with an ac field of amplitude $H_{ac}$ = 300 A/m (3.75 Oe) and zero external field. The inset shows the effects of an external dc field on the response of C1 ($f$ = 5 Hz). In the lower graph, the squares are the imaginary component of the susceptibility of C2 measured at 5 Hz.

magnetic field. A similar behaviour is found for sample C2, but another weak maximum appears in $\chi'$ at $T$ = 18.8 K, with also the out-of-phase component $\chi''$ having a maximum (Fig. 5b). These observations reveal subtle changes of the spin orientation in the magnetic structure of the Cu sublattice, in a similar way to the effects on ac susceptibility observed by Klamut [23] between 7 K and 10 K. The origin of these anomalies is still not clear. They could be related with the competition, in that temperature range, between the antiferromagnetic arrangement in the Cu sublattice and the Gd–Gd interaction. Neutron diffraction studies in $Gd_2CuO_4$ [24] have shown that the 3D magnetic order of the Cu sublat-

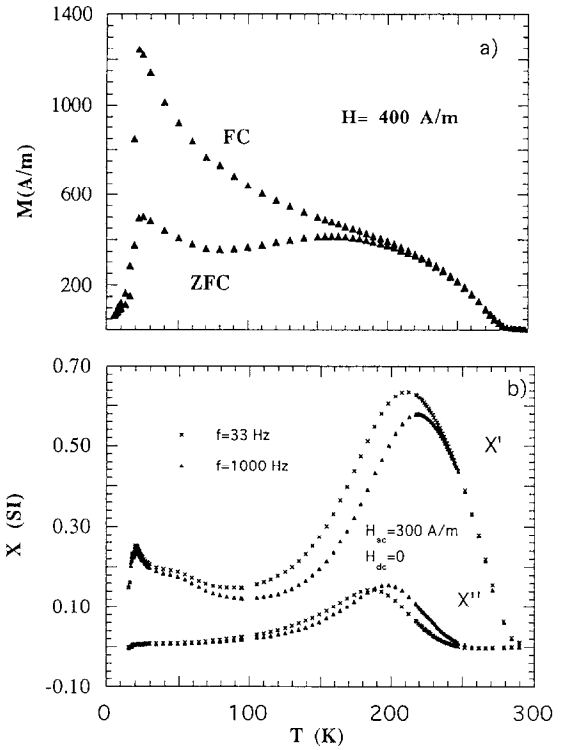


Fig. 6. (a) Dc magnetization for sol–gel sample S1 at a field of 400 A/m (5 Oe). (b) Real ( $\chi'$ ) and imaginary ( $\chi''$ ) parts of the internal ac susceptibility measured with an ac amplitude $H_{ac} = 300$ A/m (3.75 Oe) and frequencies of $f = 10$ Hz and $f = 1000$ Hz.

tice disappears in that temperature range. The competition of the Cu AF arrangement with the Gd one, which is coupled with the WF components in the

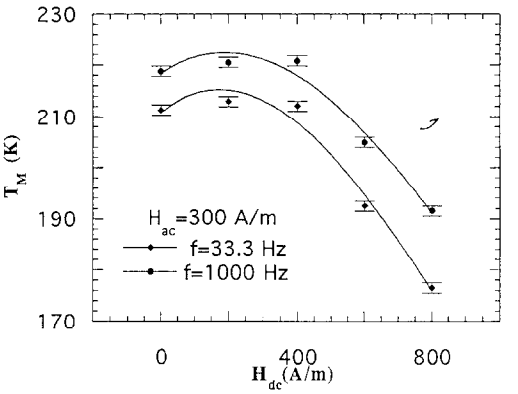


Fig. 8. Dependence of $T_M$ on $H_{dc}$ for S1.

$CuO_2$ planes [20], has been pointed out as the cause of the breaking of the 3D ordering [24].

As illustrated in Fig. 6, the ac susceptibility of the sample synthesized by the sol–gel method at 950°C (sample S1) has the same qualitative behaviour as observed for sample C1 (Fig. 3), with two anomalies in $\chi'$ at 210 K ($T_M$) and 20 K ($T_1$), but the susceptibility values are smaller in the whole investigated range and a change of slope appears at about 50 K. The maximum at $T_M$ changes its shape and value under an applied dc field, vanishing for a value $H_{dc}$ of about 700 A/m (8.75 Oe). In Fig. 7 we see the decrease of the ac amplitude versus the superimposed dc field, which causes also a shift on $T_M$ (Fig. 8). It is worth mentioning that a field of this order of magnitude is needed to eliminate the differences

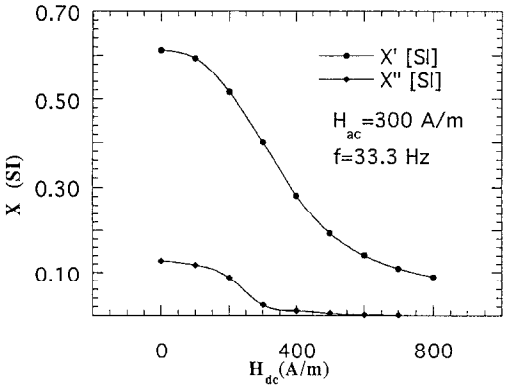


Fig. 7. Dependence of $\chi'$ at $T = 198.5$ K and $f = 33.3$ Hz on $H_{dc}$ for S1.

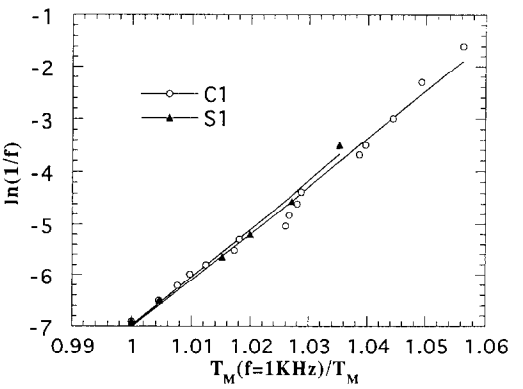


Fig. 9. Arrhenius plot showing the dependence on the frequency $f$ of $T_M$ for ceramic sample C1 and the biggest sol–gel sample, S1.

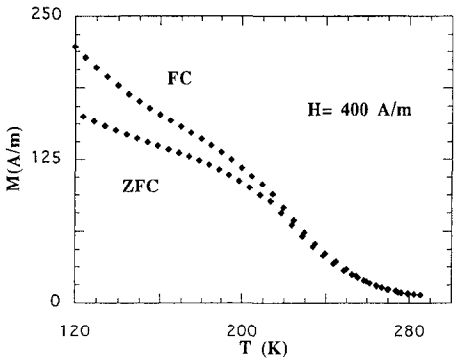


Fig. 10. Dc magnetization for sample S2 in the high temperature range at a field of 400 A/m (5 Oe).

between FC and ZFC magnetization curves in the vicinity of $T_B$. $T_M$ for S1 has a field and frequency dependence very similar to those of C1. The frequency of the ac driving field affects $T_M$ for S1 in the same way as for sample C1. This is shown in Fig. 9, where an Arrhenius plot for the frequency dependence of $T_M$ for C1 and S1 is given.

For the sol–gel samples, large changes on the magnetic properties of $Gd_2CuO_4$ are observed versus the grain size, as previously reported [16]. In the high temperature range they basically consist in the shift of $T_h$ first, as seen in Fig. 10 for S2. Reducing even more the size, both $T_B$ and $T_M$ shift to lower temperatures and the $\chi'$ maximum is reduced to a broad hump (see Fig. 11), up to the disappearance of all the WF signatures for the sample with smaller size. In the low temperature range, except for S5 where no WF signals are present, $T_l$ is almost unaffected by the frequency of the ac driving field. Increasing the frequency from 33.3 Hz to 1000 Hz causes $T_l$ to shift no more than 0.2 K for S1, while a reduction of about 0.8 K is observed for S3. The application of an external magnetic field has also a very small effect. It can be attributed, in the light of the phase diagram proposed in Ref. [14] for these temperatures, to the shift of the boundary from the WF phase to the AF one after the spin reorientation taking place at $T_l$. Only a slight increase of about 0.1 K is observed for $T_l$ as $H_{dc}$ is increased from 0 to 800 A/m (10 Oe). Besides, the value of $\chi'$ at $T_l$ is slightly depressed by $H_{dc}$. It decreases smoothly up to about 2% of the value measured at zero field for $H_{dc} = 800$ A/m (10 Oe). We note anyway, that if used the phase diagram proposed by Stepanov et al. [14] the fields are too small to observe such variations. The details of the $\chi'$ component obtained for the sol–gel samples in the temperature range between 15 K and 23 K (Fig. 12) show that the double peak structure, present in all the ceramic samples, as

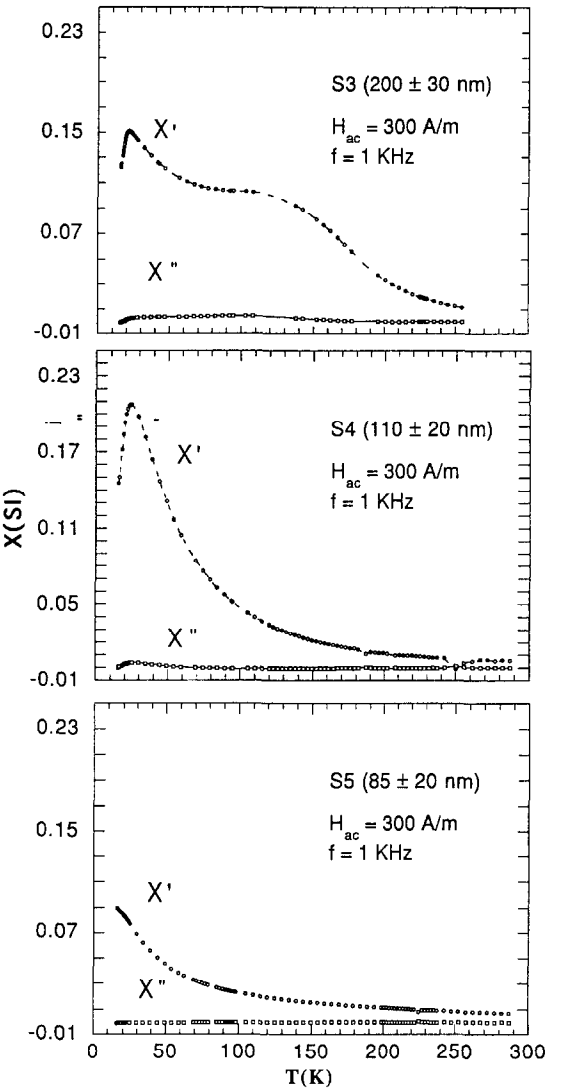


Fig. 11. Real part of the ac magnetic susceptibility of S3, S4 and S5.

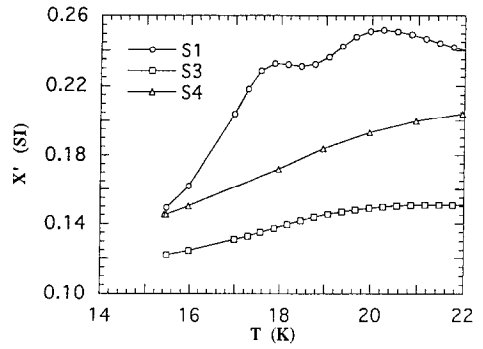


Fig. 12. Detail, at low temperatures, of the real part of the ac magnetic susceptibility for samples S1, S3 and S4; $H_{ac} = 300$ A/m (3.75 Oe), $f = 1$ kHz, $H_{dc} = 0$.

well as for the larger particle size sol–gel sample (S1), disappears as the size is reduced.

## 4. Discussion

The basic changes on the magnetic properties of $Gd_2CuO_4$ induced by different synthesis conditions appear mainly in the high temperature range, and can be separated into two types which will be shown to have their origins in two different aspects: structural and size effects. The first ones consist in the variation on the dynamic properties, which are revealed by a depression of the splitting temperature between FC and ZFC magnetizations and by a similar behaviour of $T_M$ obtained by ac susceptibility measurements. No frequency dependence was observed for sample C2, for which $T_M$ is similar to $T_h$ measured by dc magnetization, contrary to the other samples. This marks the phase transition character of $T_h$. The equivalence of $T_M$ and $T_B$ suggests that a blocking type process expected for a system of magnetic clusters or domains occurs. For such domains, a size of the order of 200 nm has been calculated for the ceramic sample annealed at the lower temperature [16]. As it is clear from the inspection of the SEM micrographs the mean particle size ranges in the ceramic samples are far over this value. Therefore, we expect that the size variations in the ceramic samples will not affect the dynamic properties because the grain size is in all the cases much greater than the domain one, i.e., variations on the domains cannot arise from this effect. The possible explanation for the observed phenomena must then be found in structural aspects. As proposed by Stepanov et al. [14], the coherence of the O(1) distortion is the main feature that gives rise to 'macroscopic WF'. The different synthesis temperature appears then as the possible source of altering these coherent distorted regions that define a certain WF domain structure.

The second type of change with the synthesis conditions is the variation of $T_h$ (the temperature associated with the 3D order of the Cu sublattice in a bulk material, $T_N$) observed in the sol–gel samples with grain sizes below 200–300 nm. When the particle size reaches this value $T_h$ begins to drop. In these compounds, the high coupling constant between the Cu moments in the $CuO_2$ planes causes two dimensional (2D) AF correlations to appear at high temperatures. These 2D correlations develop as the temperature decreases until the interaction of neighbouring $CuO_2$ planes leads to the 3D ordering [4,6,25]. Then, alterations of this 2D correlation length should imply alterations of the 3D ordering temperature, $T_N$. The particle size limit could reduce directly these correlations. From neutron diffraction studies in some $R_2CuO_4$ compounds correlation lengths from $250a$ to $100a$ have been derived [25], $a$ being the distance between adjacent Cu moments in the $CuO_2$ planes. In our case this implies distances of 100–50 nm. Sample S8, with a mean particle size of 85 nm does not show any WF signature at all, which we interpret as the elimination of the 3D AF order in the Cu sublattice. As a weak ferromagnet can be viewed as a canted antiferromagnet, the suppression of the latter gives the suppression of the former. Of course this effect is the dominant one at the smaller particle size ranges and affects the dynamic properties whenever the reduced $T_N$ is smaller than the $T_B$ associated to a given domain size, imposed by the coherent distorted zones or by the particle limits.

The structural effects seem to act basically in the ceramic samples and the size effects in the sol–gel samples. The link of both is found for the sol–gel samples with larger grain size. The fact that the magnetic behaviour of sample S1 is quite similar to the one of sample C1, in spite of their grain sizes are very different, indicates that for grain sizes above 350 nm the dynamic properties are not affected. Size effects begin to be the dominant for $\sim 250$ nm and

smaller in sol–gel samples. From S1 to S2 $T_B \sim T_M$ remains more or less unaltered whereas $T_h$ begins to decrease, indicating that the domain size is more or less constant, and smaller than the particle sizes. When the particle size becomes of the order of the WF domain size imposed by the synthesis temperature, the grain limit will define directly the WF domain volume, with the subsequent reduction of the associated blocking temperature $T_B \sim T_M$.

Finally, concerning the low temperature range, all these aspects do not affect $T_1$ in the same way. Anyway, some slight variations must be considered. First we see from the comparison of Fig. 5a and 5b that reducing the synthesis temperature in the ceramic samples implies a less complex behaviour in this zone. In the sol–gel samples this tendency is continued, as only for the bigger size ones the double peak structure is maintained (Fig. 12). The origin of this anomaly is a reorientation of the Cu sublattice due to the interaction with the Gd one. The Gd sublattice, which goes to a global AF order at 6.8 K, is polarized by the weak ferromagnetic component in the $CuO_2$ planes, $m_{Cu}$. At low temperatures the Gd–Gd interaction begins to grow, establishing a competition with the Gd–$m_{Cu}$ one that gives rise to the spin reorientation at $T_1$. The intensity of the Gd–$m_{Cu}$ interaction should be affected by the domain structure in the $CuO_2$ planes, whose effects could be the observed ones. A shift of $T_1$ to higher temperatures would be expected considering that the formation of several WF domains in the $CuO_2$ planes hinders a coherent sum of all the local WF components polarizing the Gd sites.

## 5. Conclusions

The magnetic properties of $Gd_2CuO_4$ are found to be strongly dependent on the synthesis conditions. For ceramic samples, a different annealing temperature defines local coherent-oxygen-distorted regions in the $CuO_2$ planes (understanding coherence as the property allowing a unique WF component). As the synthesis temperature is increased the extension of these regions increases, and so does therefore the size of the associated WF domains. This is measured by a change in the splitting temperature between FC and ZFC magnetizations as well as in the associated maximum in ac susceptibility measurements, $T_B$ and $T_M$.

For sol–gel samples, with different particle sizes, a change in the WF character itself occurs below 250 nm, with a diminution of WF signatures, but without altering $T_M$ and $T_B$ until a value of $\approx 200$ nm is achieved. Below this value $T_M$ and $T_B$ also decrease. The limited particle sizes could be acting directly on the 2D spin correlation length of the Cu AF arrangement and forcing a decrease of the 3D ordering temperature. This reduction of the AF global order leads to a similar reduction of WF in the material. The size control could also limit the WF domain extension under 200 nm, generating the drop of $T_M$ and $T_B$.

## Acknowledgements

We wish to acknowledge financial support from the DGICYT, Grant No. PB93-0540; Fundación Ramón Areces; NSF-DMR-91172122; and NATO, Grant No. GRG920255. JM and CV also thank Fundación Segundo Gil Dávila and Xunta de Galicia for their financial support.

## References

[1] Y. Tokura, H. Takagi and S. Uchida, Nature 337 (1989) 345; J.T. Markert, E.A. Early, T. Bjornholm, S. Ghamaty, B.W. Lee, J.J. Nuemeier, R.D. Price, C.L. Seaman, M.B. Maple, Physica C 158 (1989) 178.

[2] B. von Grande, H. Muller-Buschbaum and M. Schweizer, Z. Anorg. Allg. Chem. 428 (1977) 120.

[3] P. Bordet, J.J. Capponi, C. Chaillout, D. Chateigner, J. Chenavas, Th. Fournier, J.L. Hodeau, M. Marezio, M. Perroux, G. Thomas and A. Varela Losada, Physica C 193 (1992) 178.

[4] T.R. Thurston, M. Matsuda, K. Kakurai, K. Yamada, Y. Endoh, R.J. Birgeneau, P.M. Gehring, Y. Hidaka, M.A. Kastner, T. Murakami and G. Shirane, Phys. Rev. Lett. 65 (1990) 263.

[5] G. Shirane et al., Phys. Rev. Lett. 59 (1987) 1613; Y. Endoh et al., Phys. Rev. B 37 (1988) 7443; G. Aeppli et al., Phys. Rev. Lett. 62 (1989) 2052; R.R.P. Singh et al., Phys. Rev. Lett. 62 (1989) 2736.

[6] K. Yamada, K. Kakurai, Y. Endoh, T.R. Thurston, M.A. Kastner, R.J. Birgeneau, G. Shirane, Y. Hidaka and T. Murakami, Phys. Rev. B 40 (1990) 4557.

[7] Y. Endoh, M. Matsuda, K. Yamada, K. Kakurai, Y. Hidaka, G. Shirane and R.J. Birgeneau, Phys. Rev. B 40 (1989) 7023;

J.W. Lynn, I.W. Sumarlin, S. Shantakumar, W.-H. Li, R.N. Shelton, J.L. Peng, Z. Fisk and S.-W. Cheong; Phys. Rev. B 41 (1990) 2569; S. Shantakumar, J.W. Lynn, J.L. Peng and Z.Y. Li, J. Appl. Phys. 69 (1991) 4866.

[8] S.B. Oseroff, D. Rao, F. Wright, D.C. Vier, S. Schultz, J.D. Thompson, Z. Fisk, S.-W. Cheong, M.F. Hundley and M. Tovar, Phys. Rev. B 41 (1990) 1934.

[9] J.T. Markert, E.A. Early, T. Bjornholm, S. Ghamaty, B.W. Lee, J.J. Neumeier, R.D. Price, C.L. Seaman and M. B. Maple, Physica C 158 (1989) 178.

[10] I. Dyzaloshinskii, J. Phys. Chem. Phys. Solids 4 (1958) 241; T. Moriya, Phys. Rev. 120 (1960) 91.

[11] L.B. Steren, M. Tovar and S.B. Oseroff, Phys. Rev. B 46 (1992) 2874.

[12] Ph. Galez, P. Schweiss, G. Collin, R. Bellissent, J. Less-Common Metals 164–165 (1990) 784; R.D. Zysler, M. Tovar, C. Rettori, D. Rao, H. Shore, S.B. Oseroff, D.C. Vier, S. Schultz, Z. Fisk and S.-W. Cheong, Phys. Rev. B 44 (1991) 9467; T. Adelmann, R. Ahrens, G. Czjzek, G. Roth, H. Schmidt and C. Steinleitner, Phys. Rev. B 46 (1992) 3619; M.L. Laguna, M.L. Sanjuan, A. Butera, M. Tovar, Z. Fisk and P. Canfield, Phys. Rev. B 48 (1993) 7565.

[13] M. Braden, W. Paulus, A. Cousson, P. Vigoureux, G. Heger, A. Goukassov, P. Bourges and D. Petitgrand, Europhys. Lett. 25 (1994) 625.

[14] A.A. Stepanov, P. Wyder, T. Chattopadhyay, P.J. Brown, G. Filion, I.M. Vitebsky, A. Deville, G. Gaillard, S.N. Barilo and D.I. Zhigunov, Phys. Rev. B 48 (1993) 12979.

[15] J. Mira, J. Castro, J. Rivas, D. Baldomir, C. Vázquez-Vázquez, J. Mahia, M.A. López-Quintela, D. Fiorani, R. Caciuffo, D. Rinaldi, T. Jones and S.B. Oseroff, J. Appl. Phys. 76 (1994) 7034.

[16] J. Mira, J. Rivas, D. Fiorani, R. Caciuffo, D. Rinaldi, C. Vázquez-Vázquez, J. Mahía, M.A. López-Quintela and S.B. Oseroff, Phys. Rev. B 52 (1995) 16020.

[17] J. Mahía, C. Vázquez-Vázquez, M.I. Basadre Pampín, J. Mira, M.A. López-Quintela, J. Rivas and S.B. Oseroff, J. Am. Ceram. Soc. 79 (1996) 407.

[18] J. Mahía, A. Vieiro, J. Mira, M.A. López-Quintela, J. Rivas and S.B. Oseroff, J. Solid State Chem. (in press).

[19] J.D. Thompson, S.-W. Cheong, S.E. Brown, Z. Fisk, S.B. Oseroff, M. Tovar, D.C. Vier and S. Schultz, Phys. Rev. B 39 (1989) 6660.

[20] A. Fainstein, M. Tovar and Z. Fisk, J. Phys. Condens. Matter 4 (1992) 1581.

[21] J. Mira, J. Castro, J. Mahia, C. Vázquez-Vázquez, M.A. López-Quintela, J. Rivas and S.B. Oseroff, J. Non-Cryst. Solids 172–174 (1994) 491.

[22] M. Tovar, X. Obradors, F. Pérez, S.B. Oseroff, R.J. Duro, J. Rivas, D. Chateigner, P. Bordet and J. Chenavas, J. Appl. Phys. 70 (1991) 6095; Phys. Rev. B 45 (1992) 4729.

[23] P.W. Klamut, Phys. Rev. B 50 (1994) 13009.

[24] T. Chattopadhyay, P.J. Brown and B. Roessli, J. Appl. Phys. 75 (1994) 6816.

[25] M. Matsuda, K. Yamada, K. Kakurai, H. Kadowaki, T.R. Thurston, Y. Endoh, Y. Hidaka, R.J. Birgeneau, M.A. Kastner, P.M. Gehring, A.H. Moudden and G. Shirane, Phys. Rev. B 42 (1990) 10098.